J|A|C|S
ARTICLES

Published on Web 04/25/2008

Quantitative Lid Dynamics of MDM2 Reveals Differential Ligand Binding Modes of the p53-Binding Cleft

Scott A. Showalter, Lei Bruschweiler-Li, Eric Johnson, Fengli Zhang, and Rafael Brüschweiler*

Department of Chemistry and Biochemistry, National High Magnetic Field Laboratory, Florida State University, Tallahassee, Florida 32306

Received January 9, 2008; E-mail: bruschweiler@magnet.fsu.edu

Abstract: The oncoprotein MDM2 regulates the activity and stability of the tumor suppressor p53 through protein–protein interaction involving their N-terminal domains. The N-terminal lid of MDM2 has been implicated in p53 regulation; however, due to its flexible nature, limited data are available concerning its role in ligand binding. The quantitative dynamics study using NMR reported here shows, for the first time, that the lid in apo-MDM2 slowly interconverts between a "closed" state that is associated with the p53-binding cleft and an "open" state that is highly flexible. Our results reveal that apo-MDM2 predominantly populates the closed state, whereas the p53-bound MDM2 exclusively populates the open state. Unlike p53 binding, the small molecule MDM2 antagonist nutlin-3 binds to the cleft essentially without perturbing the closed lid state. The lid dynamics thereby represents a signature for the experimental and virtual screening of therapeutic antagonists that target the p53−MDM2 interaction.

Introduction

p53 suppresses tumor formation by inducing cell-cycle arrest, apoptosis, and senescence upon cellular stress.[1,2] Under normal conditions, p53 is maintained at a low level by MDM2 through an autoinhibitory feedback loop.[3] In this feedback loop, p53 increases the transcription level of MDM2, which in turn binds to the p53 transactivation domain to block the transactivation of its downstream genes including the mdm2 gene and, at the same time, to target p53 for proteasome degradation with its E3 ubiquitin ligase activity. In a variety of malignant human tumors p53 activity is inhibited by overexpression of MDM2.[4] Understanding of the complex formation of MDM2 with p53 as well as with other ligands is therefore of central importance for the elucidation of the p53 regulatory mechanism and for the development of antagonists that disrupt the complex for use as anticancer drugs.

MDM2 and p53 interact through their N-terminal domains. The crystal structure[5] of the N-terminal domain of MDM2 in complex with p53, where p53 is represented by a peptide, shows that MDM2 exhibits a deep hydrophobic binding cleft that accommodates three deeply buried amino acid side chains of p53 (Figure 1). The fact that the p53−MDM2 interaction is dominated by only a few amino acids suggests that the MDM2:p53 complex can be efficiently targeted by small molecule antagonists, which led to the development of a number of antagonistic drug leads, including nutlin-3.[6] Virtual drug screening identified additional antagonists including one that takes advantage of the flexibility of the binding cleft floor.[7]

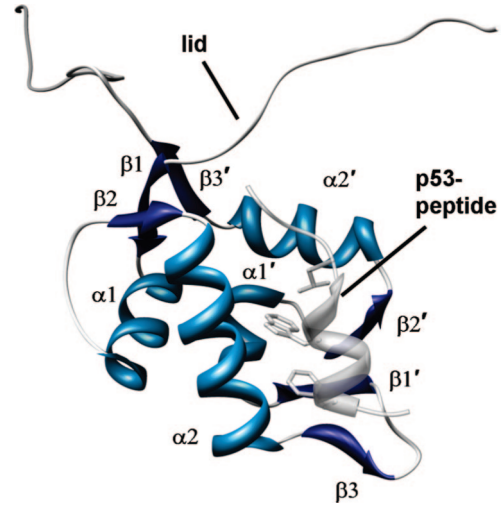

Figure 1. Ribbon diagram of the N-terminal domain of MDM2 (residues 17–125) (blue helices, purple sheets, white loops) with labels of the secondary structure elements, shown together with the bound p53 peptide (gray) based on the crystal structure of the complex (PDB code 1YCR).[5] Residues in the N-terminal "lid" of the domain were not assigned a conformation in the crystallographic structure determination[5] and are indicated in an extended conformation consistent with the NMR data described in the text.

(1) Levine, A. J. *Cell* **1997**, *88*, 323–331.
(2) Römer, L.; Klein, C.; Dehner, A.; Kessler, H.; Buchner, J. *Angew. Chem., Int. Ed.* **2006**, *45*, 6440–6460.
(3) Harris, S. L.; Levine, A. J. *Oncogene* **2005**, *24*, 2899–2908.
(4) Bond, G. L.; Hu, W. W.; Levine, A. J. *Curr. Cancer Drug Targets* **2005**, *5*, 3–8.
(5) Kussie, P. H.; Gorina, S.; Marechal, V.; Elenbaas, B.; Moreau, J.; Levine, A. J.; Pavletich, N. P. *Science* **1996**, *274*, 948–953.
(6) Vassilev, L. T.; Vu, B. T.; Graves, B.; Carvajal, D.; Podlaski, F.; Filipovic, Z.; Kong, N.; Kammlott, U.; Lukacs, C.; Klein, C.; Fotouhi, N.; Liu, E. A. *Science* **2004**, *303*, 844–848.
(7) Bowman, A. L.; Nikolovska-Coleska, Z.; Zhong, H. Z.; Wang, S. M.; Carlson, H. A. *J. Am. Chem. Soc.* **2007**, *129*, 12809–12814.

10.1021/ja800201j CCC: $40.75

The N-terminal flexible lid of MDM2 consisting of residues 19 – 24 of MDM2, which is not resolved in the MDM2:p53 crystal structure, has been suggested to partially bind to the p53-binding cleft of apo-MDM2 based on NMR chemial shifts.[8] This led to the implication of p53 regulation by phosphorylation of the lid. In the NMR structure of apo-MDM2 the lid is not well-defined due to the lack of long-range NOEs.[9] The limited amount of experimental data thereby precluded the accurate modeling of the lid and its precise binding mode to the cleft. In addition, it has been proposed that the binding event induces global conformational changes of MDM2, which would have important implications for drug design.[10]

Here, we report the comprehensive, quantitative characterization of the N-terminal domain (amino acids 17–125) of human MDM2 in solution by multidimensional NMR including heteronuclear NMR spin relaxation, chemical shift analysis, and paramagnetic relaxation enhancement. A special focus is the characterization of the behavior of the lid in the apo state, the p53-bound state, and in complex with nutlin-3. Our study provides a structural dynamic picture of MDM2 in solution and its interaction with p53 and antagonistic ligands at unprecedented detail. The results show how the lid dynamics directly interfere with ligand binding and suggest how they can be used as a drug screening probe.

Experimental Section

Sample Preparation. The DNA fragment corresponding to human MDM2 amino acids 17–125 was PCR amplified from an EST clone (accession number BM479400) and cloned into the ligation independent cloning vector pTBGST (courtesy of Dr. Tim Cross), which encodes a N-terminal 6x His tag and GST protein fusion with a TEV recognition site upstream of the cloning site. Based on chemical shift analysis of the apo-form, it has been found[9] that residues 1–16 adopt a random-coil configuration and therefore were not included in the present construct. While interactions involving the remaining domains in full length MDM2 may impact the structure and dynamics of the N-terminal domain, these effects are not investigated in the current study. The resulting plasmid was introduced into the *E. coli* protein expression strain BL21(DE3). The peptide corresponding to human p53 residues 17–29 (amino acid sequence ETFSDLWKLLPEN) was synthesized using an Applied Biosystems 433A peptide synthesizer. Following synthesis, the peptide was purified on a C-18 reversed phase HPLC column and dried for storage. Nutlin-3 was purchased from Cayman Chemical Company and further purified on an (S,S)-Whelk-0 (Regis Technologies) chiral separation column. The enantiomer with greater binding activity for MDM2 was recovered and then dried for storage.

NMR samples were prepared by growing *E. coli* cultures containing $^{15}NH_4Cl$ as the sole nitrogen source and either uniform ^{12}C or ^{13}C glucose as the carbon source. Expression was induced with 0.5 mM IPTG at $OD_{600} = 0.6$, and the cells were harvested after 3 h of further growth. Ni-NTA agarose (Qiagen) was used to purify the fusion protein, and the pure MDM2(17–125) was released after TEV cleavage with the non-native residues SNA preceding the first native MDM2 residue. The purified protein was concentrated to 300 μM (below the 350 μM solubility limit) in an Amicon Ultra centrifugal filter device (Millipore) and buffer exchanged to 50 mM HEPES pH 7.0, 100 mM NaCl, and 5 mM DTT, 0.05% (w/v) NaN_3, with 10% D_2O to provide an NMR lock signal. N-terminal sequencing confirmed proper cleavage of the purified protein. Dynamic light scattering on 3 mg/mL MDM2 confirmed that the protein is monodisperse with a similar hydrodynamic radius in both the free and p53-peptide bound form. MDM2 in complex with p53 was further confirmed to be monomeric by sedimentation equilibrium analytical ultracentrifugation. Peptide bound samples were generated by adding p53 peptide in a 2:1 molar excess following concentration. Nutlin-3 bound samples were generated by adding nutlin-3 to a final concentration of 500 μM from a stock of 50 mM nutlin-3 in DMSO-d_6. MDM2 has been shown to bind nutlin-3 strongly ($K_D = 700$ nM)[11] under conditions similar to our NMR conditions, including the presence of 2% DMSO. Consistent with previous studies,[12] no change in the apo-MDM2 $^{15}N-^{1}H$ HSQC spectrum was detected here in the presence of 2% DMSO.

NMR Methods. All NMR experiments were performed at 25 °C on a Bruker Avance II 800 MHz spectrometer with a cryogenic TCI probe. Standard triple resonance NMR techniques have been used to assign >94% of the backbone of apo-MDM2 and >98% of the backbone of the MDM2:p53 and MDM2:nutlin-3 complexes. Backbone ^{15}N T_1 and heteronuclear NOE experiments were performed using previously published pulse programs[13] optimized by removing the water flip back pulse in the initial INEPT period of the T_1 and by the inclusion of pulsed field gradients to suppress radiation damping during the indirect evolution period of the heteronuclear NOE. Backbone ^{15}N $T_{1\rho}$ experiments used a pulse program analogous to scheme 2 from Massi et al.[14] in order to account for the low spin-lock field required by the cryogenic probe. The spin-lock field applied during the relaxation period was calibrated to be $\gamma_N B_1/2\pi = 0.988$ kHz. Backbone ^{15}N η_{xy} experiments were performed using a pulse program from the literature.[15] Spectral widths and carrier frequencies (in parentheses) for all relaxation experiments were set for ^{1}H to 16 ppm (4.77 ppm) and for ^{15}N to 33 ppm (118 ppm), except for the ^{15}N $T_{1\rho}$ in which the ^{15}N spectral width was set to 38 ppm and two data sets were collected with carrier frequencies of 113 and 123 ppm in order to minimize off-resonance effects. The $T_{1\rho}$ rates were corrected for off-resonance effects using the relation $T_2 = T_{1\rho}(T_1 \sin^2 \theta)/(T_1 - T_{1\rho} \cos^2 \theta)$ with $\tan \theta = \gamma_N B_1/2\pi\Delta\nu$. All relaxation experiments were acquired using synchronous GARP decoupling during acquisition to remove ridge artifacts.[16] Heating effects were minimized in all spin relaxation experiments by collecting the data as interleaved pseudo-3D spectra. The T_1 relaxation delay was sampled at eight time points: 100, 300, 500, 700, 900, 1100, 1300, and 1500 ms, with a replicate point at 300 ms for error analysis. The $T_{1\rho}$ relaxation delay was sampled at nine time points: 16, 32, 48, 64, 80, 96, 112, 128, and 144 ms, with a replicate point at 32 ms for error analysis. The η_{xy} relaxation delay was sampled at five time points: 11, 16, 21, 27, and 32 ms. The recycle delay was set to 3 s for all experiments except for the heteronuclear NOE in which a 5 s delay was used. All spectra were processed using NMRPipe[17] and analyzed in Sparky.[18]

(8) McCoy, M. A.; Gesell, J. J.; Senior, M. M.; Wyss, D. F. *Proc. Natl. Acad. Sci. U.S.A.* **2003**, *100*, 1645–1648.
(9) Uhrinova, S.; Uhrin, D.; Powers, H.; Watt, K.; Zheleva, D.; Fischer, P.; McInnes, C.; Barlow, P. N. *J. Mol. Biol.* **2005**, *350*, 587–598.
(10) Schon, O.; Friedler, A.; Freund, S.; Fersht, A. R. *J. Mol. Biol.* **2004**, *336*, 197–202.
(11) Popowicz, G. M.; Czarna, A.; Rothweiler, U.; Szwagierczak, A.; Krajewski, M.; Weber, L.; Holak, T. A. *Cell Cycle* **2007**, *6*, 2386–2392.
(12) D'Silva, L.; Ozdowy, P.; Krajewski, M.; Rothweiler, U.; Singh, M.; Holak, T. A. *J. Am. Chem. Soc.* **2005**, *127*, 13220–13226.
(13) Brutscher, B.; Brüschweiler, R.; Ernst, R. R. *Biochemistry* **1997**, *36*, 13043–13053.
(14) Massi, F.; Johnson, E.; Wang, C. Y.; Rance, M.; Palmer, A. G. *J. Am. Chem. Soc.* **2004**, *126*, 2247–2256.
(15) Hall, J. B.; Fushman, D. *Magn. Reson. Chem.* **2003**, *41*, 837–842.
(16) van Ingen, H.; Vuister, G. W.; Tessari, M. *J. Magn. Reson.* **2002**, *156*, 258–261.
(17) Delaglio, F.; Grzesiek, S.; Vuister, G. W.; Zhu, G.; Pfeifer, J.; Bax, A. *J. Biomol. NMR* **1995**, *6*, 277–293.
(18) Goddard, T. D.; Kneller, D. G. *SPARKY 3;*, University of California, San Francisco: 2003.
(19) Mandel, A. M.; Akke, M.; Palmer, A. G. *J. Mol. Biol.* **1995**, *246*, 144–163.

Model-free Analysis. Lipari−Szabo model-free fitting was performed using the program ModelFree 4.15,[19] with diffusion tensor fitting performed using the quadric method.[20,21] Residues identified as exchanging on the microsecond−millisecond time scale by their η_{xy}/R_2 ratio were excluded from analysis in determining the overall diffusion tensor. The coordinates of MDM2 from the co-crystal structure[5] were used as a structural reference for diffusion tensor determination in both the free and bound states. For each residue in the core domain of MDM2 (residues 25–109), T_1, T_2, and NOE data were fit to a model including the axially symmetric global diffusion parameters with S^2 and τ_{int} to model internal motions or S^2 and R_{ex} for those residues identified as undergoing exchange according to their η_{xy}/R_2 ratio.

Paramagnetic Relaxation Enhancement (PRE). Samples for paramagnetic relaxation enhancement were prepared as described and 4-hydroxy-TEMPO (TEMPOL) (Sigma-Aldrich) was added to a final concentration of 5 mM. PRE spectra were collected with in-house written pulse programs consistent with the one by Clore et al.,[22] and data were fit to eq 1:[22]

$$\Gamma_2 = R_{2,\mathrm{para}} - R_{2,\mathrm{dia}} = \frac{1}{T_{\Delta T} - T_0} \ln\left[\frac{I_{\mathrm{dia}}(T_{\Delta T}) I_{\mathrm{para}}(T_0)}{I_{\mathrm{dia}}(T_0) I_{\mathrm{para}}(T_{\Delta T})}\right] \quad (1)$$

where $R_{2,\mathrm{para}}$ and $R_{2,\mathrm{dia}}$ are the transverse relaxation rates R_2 in paramagnetic and diamagnetic solution, respectively, $I(T)$ is the peak intensity at time T under the conditions indicated, and T_0 and $T_{\Delta T}$ are the short and long delay time points, respectively. For the present study $T_0 = 0$ ms and $T_{\Delta T} = 30$ ms were used.

Results and Discussion

Apo-MDM2 Exists in Two States: Major (Dominant or Closed) and Minor (Open). Solution conditions were optimized to obtain adequate solubility (350 μM) and high sample stability (>1 month) for both the apo and bound states of MDM2, representing an improvement over previous studies.[8–10,23,24] Sedimentation equilibrium analytical ultracentrifugation measurements show that MDM2 is monomeric under these conditions. These conditions allowed the collection of high quality NMR data at a high magnetic field using a cryogenically cooled probe for the accurate determination of T_1, T_2, NOE data, and chemical shifts. Comparison of ^{15}N−^{1}H HSQC NMR spectra of apo-MDM2 and the MDM2:p53 complex show that the major differences in chemical shift are observed in the vicinity of the binding cleft, with the largest changes involving the lid and strand β1 (see Supporting Information Figure 1). Furthermore, secondary C$^\alpha$ and CO chemical shifts show only small changes (Supporting Information Figure 3) indicating that p53 binding does not affect the lengths and composition of individual secondary structural elements.

For the first time two distinct sets of HSQC peaks were identified for apo-MDM2 for each of the residues in the lid with the major set constituting 90% of the total apo-MDM2 as determined by peak volume comparison (Figure 2). The residues possessing two sets of peaks are I19, P20 (two sets of ^{13}C resonances in the triple resonance data, both consistent with a *trans* peptide bond), A21, S22, and E23. The resonances of the minor set of these residues have chemical shifts that are very similar to the ones of the p53-bound form of the lid (red resonances, Figure 2), whereas the major set of peaks show significant chemical shift differences with respect to the MDM2:p53 complex. These findings demonstrate the presence of a slow dynamic equilibrium on the >10-ms time scale between a dominant and a minor state of the lid, which in the following is further structurally and dynamically characterized by secondary chemical shifts, paramagnetic relaxation, and ^{15}N spin relaxation measurements.

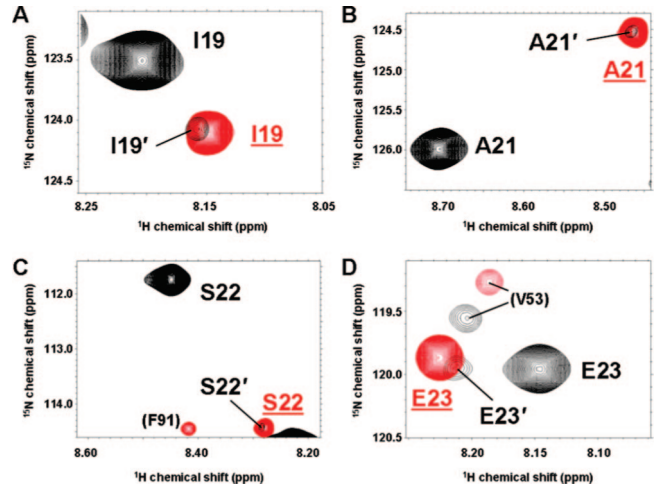

Figure 2. Observation of two distinct conformational substates of the apo-MDM2 N-terminal lid (residues 19–23). (A−D) sections of the ^{15}N−^{1}H HSQC spectrum corresponding to lid residues for apo-MDM2 (black) and the MDM2:p53 complex (red). HSQC peaks of the MDM2 lid are observed for a major conformer and a minor conformer (primed label). Only one lid conformer is observed in the MDM2:p53 complex, with its peak position coinciding with that of the minor apo-conformer. Additional resonances in the HSQC sections are labeled with their assignments in parentheses.

Helical Lid Structure of the Major apo-MDM2 State Becomes Disordered in MDM2:p53. In the major apo-MDM2 state, elevated secondary ^{13}C chemical shifts observed for the lid residues A21, S22, E23, and Q24 (Figure 3A,B) and small backbone $^{3}J(H^N,H^\alpha)$-scalar couplings (Figure 3C) suggest strong α-helical propensity, which is consistent with previous findings.[8] By contrast, the small secondary chemical shifts measured for these residues in the minor apo-state and the p53-bound state imply a disordered state, which is consistent with their increased backbone scalar $^{3}J(H^N,H^\alpha)$-couplings observed for the p53-bound state. This suggests that the α-helical conformation of the lid may be induced upon association with the binding cleft, in analogy to the induced helix of the p53 peptide.[25] The α-helical lid state is only marginally stable as it can be destabilized by the addition of relatively small quantities of urea (500 mM, see Supporting Information Figure 2).

Lid in the Dominant apo-MDM2 State Is Binding Cleft Associated. It is well-known that helical protein lids (e.g., that of lipase[26]) can participate in governing ligand binding by interacting with the active site in the apo-state. To further elucidate the relative position of the MDM2 lid with respect to the binding cleft, i.e. the core domain of MDM2, relaxation enhancement measurements in the presence of paramagnetic radicals were performed. Such measurements provide distance

(20) Brüschweiler, R.; Liao, X. B.; Wright, P. E. *Science* **1995**, *268*, 886–889.
(21) Lee, L. K.; Rance, M.; Chazin, W. J.; Palmer, A. G. *J. Biomol. NMR* **1997**, *9*, 287–298.
(22) Iwahara, J.; Tang, C.; Clore, G. M. *J. Magn. Reson.* **2007**, *184*, 185–195.
(23) Stoll, R. et al. *Biochemistry* **2001**, *40*, 336–344.
(24) Schon, O.; Friedler, A.; Bycroft, M.; Freund, S. M. V.; Fersht, A. R. *J. Mol. Biol.* **2002**, *323*, 491–501.
(25) Dawson, R.; Muller, L.; Dehner, A.; Klein, C.; Kessler, H.; Buchner, J. *J. Mol. Biol.* **2003**, *332*, 1131–1141.
(26) Brzozowski, A. M.; Derewenda, U.; Derewenda, Z. S.; Dodson, G. G.; Lawson, D. M.; Turkenburg, J. P.; Bjorkling, F.; Huge-Jensen, B.; Patkar, S. A.; Thim, L. *Nature* **1991**, *351*, 491–494.

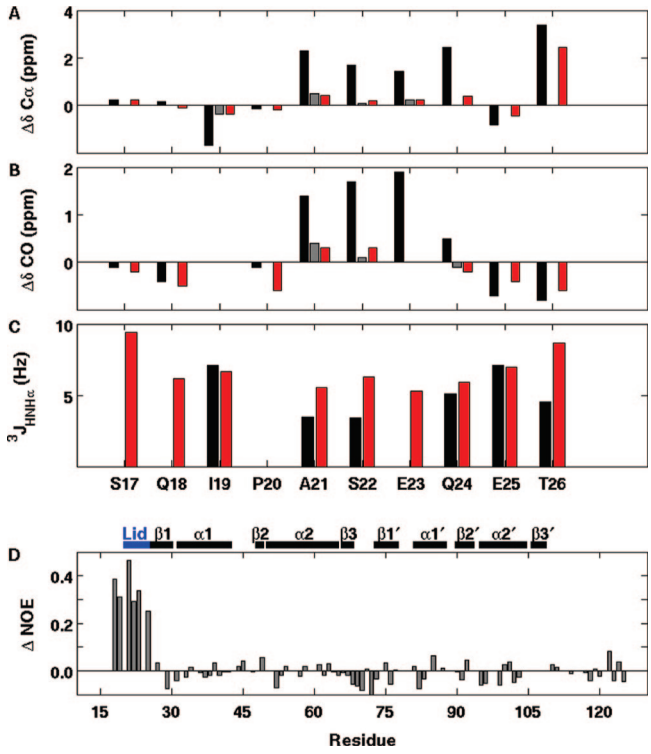

Figure 3. The major lid conformation is structurally and dynamically altered by p53 binding. (A,B) Deviation of the $^{13}C^{\alpha}$ and ^{13}CO chemical shifts of the N-terminal MDM2 residues from their residue specific random coil values. Strongly positive values are consistent with an α-helical conformation and near zero values with random coil. (C) $^3J(H^N,H^{\alpha})$ scalar couplings for N-terminal MDM2 residues, with values of ~5 Hz indicating α-helical conformation. Black, gray, and red bars in panels A−C correspond to the dominant conformation in apo-MDM2, minor conformation of apo-MDM2, and the MDM2:p53 complex, respectively. (D) $\{^1H\}-^{15}N$ NOE represented by residue as $\Delta NOE = NOE_{apo,closed} - NOE_{p53\text{-}bound}$. The strong positive ΔNOEs of the lid residues indicate a significantly more ordered conformation in the dominant apo-MDM2 state than that in the MDM2:p53 complex.

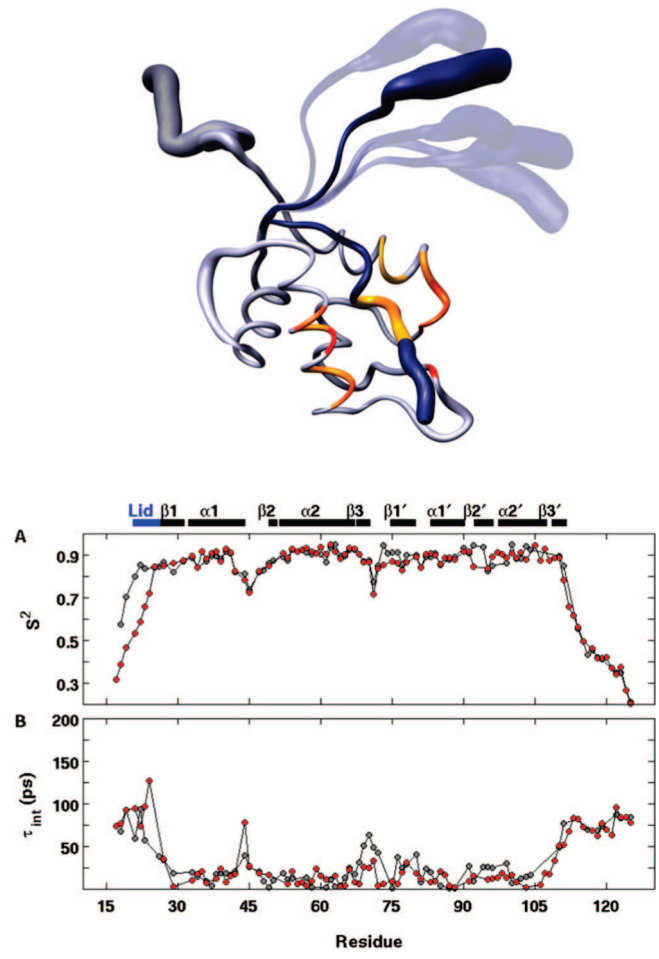

Figure 4. The lid in the minor state is not associated with the cleft and is more dynamic than in the dominant state. Mapped in orange on the model of closed MDM2 is the TEMPOL induced paramagnetic relaxation, with progression from yellow to red indicating stronger $^1H^N$ relaxation enhancement. The minor apo- and p53-bound states show no effect in the lid by the presence of TEMPOL, indicating that in these state the lid is placed away from the cleft. (A,B) Backbone amide S^2 order parameters and internal correlation times τ_{int} for the backbone amides of (dominant) apo- and p53-bound MDM2 (gray and red, respectively). The amplitude of dynamics in the N-terminus and lid on the picosecond−nanosecond time scale is substantially reduced for the dominant substate of apo-MDM2 compared with the p53-bound state.

information up to 10 Å and allow detailed studies of transient complexes.[27] The paramagnetic radical TEMPOL used here has a propensity for associating with hydrophobic patches on protein surfaces.[28] Indeed, it is found to induce paramagnetic relaxation in α2, *β1′*, *β2′*, and α2′ near the p53 residue W23 side-chain binding pocket of apo-MDM2 (Figure 4, orange residues in the ribbon diagram). Paramagnetic relaxation enhancement is not present in the corresponding region in the p53-bound state most likely because p53 peptide blocks TEMPOL access to the binding cleft (see Supporting Information Figure 4). Importantly, the dominant apo-state shows clear TEMPOL induced paramagnetic relaxation for residues Q18−A21 of the lid as depicted in Figure 4, suggesting a close interaction of the lid with the binding cleft in this state. In contrast, the minor apo-state shows no relaxation enhancement in Q18−A21 upon addition of TEMPOL, indicating that in this state the lid must be placed on average more than 10 Å away from the paramagnetic binding sites in the cleft. We conclude that, in this dynamic state, the lid extends into the solvent with little interaction with the binding cleft. Consistent with this result, the lid of p53-bound MDM2 shows also no response to TEMPOL addition (see Supporting Information Figure 4), implying that p53 successfully competes with the lid for association with the cleft, thereby exposing the lid to the solvent. Taken together, these findings demonstrate the presence of a slow equilibrium between a dominant closed α-helical lid state that is cleft-associated and a minor open disordered lid state that closely resembles the lid state when the p53 peptide is bound.

Dynamics Profile of MDM2. Nuclear spin relaxation is a rich source of protein dynamics information.[29–32] Here, information

(27) Tang, C.; Iwahara, J.; Clore, G. M. *Nature* **2006**, *444*, 383–386.
(28) Deschamps, M. L.; Pilka, E. S.; Potts, J. R.; Campbell, I. D.; Boyd, J. *J. Biomol. NMR* **2005**, *31*, 155–160.
(29) Eisenmesser, E. Z.; Millet, O.; Labeikovsky, W.; Korzhnev, D. M.; Wolf-Watz, M.; Bosco, D. A.; Skalicky, J. J.; Kay, L. E.; Kern, D. *Nature* **2005**, *438*, 117–121.
(30) Mittermaier, A.; Kay, L. E. *Science* **2006**, *312*, 224–228.
(31) Sugase, K.; Dyson, H. J.; Wright, P. E. *Nature* **2007**, *447*, 1021–1025.
(32) Frederick, K. K.; Marlow, M. S.; Valentine, K. G.; Wand, A. J. *Nature* **2007**, *448*, 325–329.

on picosecond−nanosecond time scale dynamics is gained from backbone ^{15}N NMR spin relaxation data.[33,34] Selected relaxation parameters of apo-MDM2 were previously reported, but no quantitative analysis was attempted.[8,9,23] A useful indicator of differential dynamics between apo and p53-bound MDM2 is the NOE difference $\Delta NOE = NOE_{apo,closed} - NOE_{p53\text{-}bound}$ shown in Figure 3D. The only regions with clearly positive ΔNOEs are the lid and the beginning of $\beta 1$ indicating that in these regions the dynamics of p53-bound MDM2 exceed those of the apo-state. This is further elucidated by a complete model-free analysis[33] of ^{15}N T_1, T_2 and $\{^1H\}-^{15}N$ NOE NMR spin relaxation data at 800 MHz field strength for both apo-MDM2 and MDM2:p53 (see Supporting Information Figure 5). In the model-free approach residue-specific amplitudes of motion are quantified in terms of a generalized order parameter S^2 (Figure 4A) and a motional time scale represented by an internal correlation time τ_{int} (Figure 4B). The global tumbling behavior is found to be significantly anisotropic with effective rotational diffusion correlation times $\tau_c = 8.61$ and 9.67 ns and diffusion anisotropies $D_{||}/D_{\perp}$ 1.38 and 1.41 for apo-MDM2 and MDM2:p53, respectively.

The model-free parameters S^2 and τ_{int} (Figure 4) reveal a characteristic dynamics profile of the MDM2 N-terminal domain in the p53-bound and the dominant apo states. In its core domain and in the C-terminal tail there is very little difference in the dynamics between the two states, except for the $\beta 1'$ and $\beta 2'$ strands located at the open end of the cleft that is furthest apart from the lid. Surprisingly, little difference is seen in the dynamics of the flexible loops connecting the secondary structural elements of the p53-binding cleft suggesting that they retain their flexibility irrespective of the binding state. In contrast, lid dynamics is dramatically altered between the two states. In the p53-bound state, a steep drop of the S^2 values toward the N-terminus is observed, which reflects significant fraying effects indicating that the lid residues reorient largely independently from the core domain. On the other hand, in the dominant apo-state the mobility of lid residues A21−E25 is much more restricted as evidenced by the absence of such a drop in S^2. Rather, in this state these residues have order parameters nearly as high as those of the core domain, indicating a much higher degree of order of the lid than that of the p53-bound state.

Nutlin-3 Binding Mode Is Distinct from That of the p53 Peptide. The spin relaxation and PRE data suggest that lid dynamics play a critical role in guarding access to the binding cleft and, through competition between self-association and external ligand binding, in determining the minimum affinity for successful binding. Recently, a class of imidazoline derived compounds referred to as nutlins have been developed as inhibitors of the MDM2:p53 interaction, which are successful in *in vivo* studies and serve as anticancer lead compounds (see Supporting Information Figure 6 for the structure of nutlin-3).[6,35] While structures of MDM2 bound to various nutlins have been solved by X-ray crystallography[6] and NMR,[36] no information is available concerning the lid behavior. Our NMR data of the MDM2:nutlin-3 complex show that in solution the lid residues of MDM2 still display two sets of peaks like in the case of apo-MDM2, which closely coincide with the peak positions

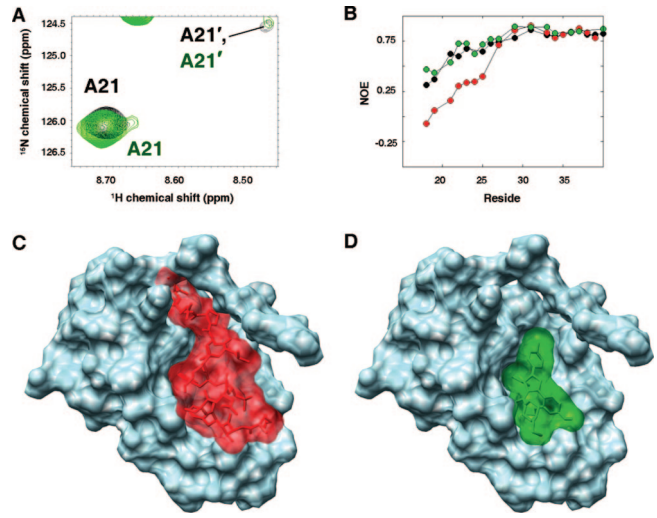

Figure 5. Nutlin-3 binds with a mechanism distinct from the p53 peptide. (A) Superposition of $^{15}N-^1H$ HSQC spectra of apo-MDM2 (black) and MDM2:nutlin-3 (green) shows that lid states in apo-MDM2 and MDM2:nutlin-3 are similar. Unlike the MDM2:p53 complex (Figure 2B), the complex with nutlin-3 contains only a small population of the open state (fully released lid). (B) $\{^1H\}-^{15}N$ NOEs of lid residues of MDM2:nutlin-3 (green) closely follow the ones of the apo-state (black) but differ from MDM2:p53 NOEs (red). (C) The surface representation of MDM2 (blue, PDB code 1YCR) bound to the p53 peptide (red) shows that the peptide and the lid must compete to occupy the top of the cleft, favoring an open conformation of the lid. (D) Nutlin-3 (green, represented by nutlin-2 from pdb 1RV1) is much more compact than the p53 peptide and binds in a configuration that does not prevent the lid from associating with the cleft.

found for apo-MDM2 (Figure 5A). In addition, peak volume analysis indicates that the population ratio between the closed and the open state is about 9:1, which is very close to that of apo-MDM2. Also similar to apo-MDM2, secondary Cα and CO chemical shift analysis reveals a helical structure in the lid (see Supporting Information Figure 3). Therefore, unlike p53 binding, nutlin binding does not shift the equilibrium of the lid state to the open dynamic form. This can be explained based on comparison of the cocrystal structures of MDM2:p53 (1YCR[5]) and MDM2:nutlin-2 (1RV1[6]) (Figure 5C, D). The volume of the p53 peptide as bound to MDM2 in the crystal structure is 1530 Å^3, whereas nutlin-2 has a volume of only 600 Å^3. In addition to being approximately 2.5 times as large by volume, the p53 peptide projects atoms much closer to the junction between the N-terminal lid and the core domain of MDM2 (Figure 5C), which precludes association of the lid with the p53 bound cleft. Nutlin-3, which is structurally very similar to the crystallized nutlin-2, fits deeply into the binding pocket, leaving considerably more of the MDM2 cleft surface exposed and accessible to association with the lid (Figure 5D). This suggests that there is no direct competition between the lid and the nutlins. Accordingly, upon nutlin binding, the $\{^1H\}-^{15}N$ NOE values of the lid residues are similar to those of apo-MDM2, in contrast to the sharp drop of the corresponding NOE values exhibited by MDM2:p53 (Figure 5B). This reflects the same reduction of motion of the lid in the nutlin-bound form and apo-MDM2 compared with the p53-bound form.

Conclusions

Adequate sample concentration and good sample stability are a prerequisite for a quantitative solution-state protein NMR study. The human MDM2 N-terminal p53-binding domain has

(33) Lipari, G.; Szabo, A. *J. Am. Chem. Soc.* **1982**, *104*, 4546–4559.
(34) Palmer, A. G. *Chem. Rev.* **2004**, *104*, 3623–3640.
(35) Vassilev, L. T. *Trends Mol. Med.* **2007**, *13*, 23–31.
(36) Fry, D. C.; Emerson, S. D.; Palme, S.; Vu, B. T.; Liu, C. M.; Podlaski, F. *J. Biomol. NMR* **2004**, *30*, 163–173.

previously been described to be unstable in solution,[9,23,37] thereby limiting NMR studies of human MDM2. This led to the use of *Xenopus*-based humanized MDM2 as an alternative system for chemical library screening by NMR.[38] The improved sample conditions for human MDM2 reported here permit for the first time a quantitative dynamics study of this protein in its apo form, in complex with p53, and with a small-ligand antagonist. This information provides the basis for improving the understanding of p53 regulation and for the design of anticancer drugs that target the MDM2−p53 interaction.

Chemical shifts, ^{15}N relaxation, and PRE data provide a highly consistent picture of the structural dynamics of MDM2 and its changes upon ligand binding to its hydrophobic cleft. Changes of the ^{15}N and H^{N}chemical shifts between the apo-state and the p53-bound state are observed for the lid and its extension into the protein core, strand β1, as well as to the vicinity of the cleft. Moreover, the small nature of C$^{\alpha}$ and CO secondary chemical shift changes reflects the preservation of all secondary structures in MDM2 upon p53 binding. This indicates that changes of structure and environment probed by chemical shifts are confined to the lid, the cleft, and their close vicinity.

The {^{1}H}−^{15}N NOEs (Figure 3) are consistent with the chemical shift results in that the main changes are observed for the lid. In addition, negative NOE changes occur in the loop region at the bottom of the cleft that connects strands β3 and β1′ (Figure 3D). A model-free analysis of the NOEs combined with ^{15}N T_1 and T_2, which disambiguates spatial from temporal dynamics effects, shows that this change is caused by a slow-down of the internal motions with internal correlation times larger than 50 ps (Figure 4B). The model-free analysis also reveals that the overall tumbling of the protein is significantly anisotropic in both the apo- and the p53-bound state and that the tumbling rate slows down by 11% when going from apo-MDM2 to MDM2:p53. Such an increase of the hydrodynamic protein volume is caused by the exposure of the lid to the solvent upon p53 binding.

The anisotropic tumbling model is critical for the adequate interpretation of dynamics. This is evident for the long helix α2 whose decreased ^{15}N $1/T_2$ rates were previously interpreted in terms of microsecond−millisecond exchange.[9] However, the quantitative anisotropic tumbling model used here fully accounts for the uniform increase of the ^{15}N T_1/T_2 ratios observed for α2 because this helix and its backbone ^{15}N−^{1}H bond vectors are roughly parallel to the symmetry axis of the prolate diffusion tensor. Inclusion of anisotropic global tumbling for the interpretation of the relaxation data used here therefore eliminates the need for slower microsecond−millisecond exchange contributions to account for the experimentally observed $1/T_2$ relaxation rates.

Except for the lid region, the S^2 order parameter profile of the two states is remarkably similar (Figure 4A). A small decrease of dynamics is observed for the apo-state in the two small parallel strands β1′ and β2′ that are part of the hydrophobic cleft.

Taken together, our results demonstrate that, with the exception of the lid and parts of the cleft, MDM2 behaves structurally and dynamically very similar in the apo- and the p53-bound states. Therefore, they do not support the previous conclusion that p53 binding induces a global conformational and dynamic change in MDM2.[10] In addition, although no crystal structure is available of the apo-state, the crystal structures of several MDM2−peptide and MDM2−small ligand complexes[5,6,39] superimpose rather well (0.87 Å backbone rmsd), which further supports the notion that the binding situation in the cleft has little effect on the rest of the protein.

The N-terminal lid of MDM2 displays differential behavior between the various binding states of MDM2. Apo-MDM2 and MDM2:nutlin-3 exhibit a dynamic equilibrium between a dominant "closed" state and a minor "open" state with an average interconversion rate constant that is slow on the chemical shift time scale as evidenced by two sets of resonances for the lid residues. MDM2:p53 on the other hand gives rise to a single set of resonances, which is nearly identical to the one of the minor state of apo-MDM2. A recent NMR study suggested that in apo-MDM2 a portion of the protein's N-terminal lid forms intramolecular contacts with the binding cleft.[8] The present study unequivocally shows that even in the apo-state the lid exists in a slowly interconverting equilibrium between the dominant closed form and a minor open form in which the lid extends away from the binding cleft, allowing a full access of ligands to the binding pocket. Interestingly, the lid behavior of the MDM2:nutlin-3 complex is similar to that of apo-MDM2 despite the fact that nutlin-3 occupies the p53-binding cleft.

Upon binding of the p53 peptide to MDM2, a disordered, high entropy form of the lid is adopted, which, compared to apo-MDM2, reflects a substantial shift in the conformational equilibrium toward the open state. The disappearance of the closed lid state involves the breakage of stabilizing interactions present between the lid and cleft residues, which are compensated mostly by hydrophobic p53−MDM2 interactions.

In contrast, binding of nutlin-3 does not release the lid from the cleft and therefore is not accompanied by the same configurational entropy increase as that for p53 binding. Nutlin-3 binding therefore appears to be predominantly enthalpy controlled. Similarly, MDM2-binding studies of a C-terminally truncated p53 peptide, which (like nutlin-3) does not occupy the narrow part of the cleft, show a more favorable binding enthalpy and 10 times stronger binding affinity than a peptide similar to the one used here ($K_D \approx 50$ nM vs 500 nM).[24] This suggests that retention of the closed lid conformation upon ligand binding preserves enthalpically favorable MDM2−lid interactions. For relatively small compounds, like the nutlins and TEMPOL, it is therefore possible to be bound without the lid being ejected and thereby to largely bypass its role in ligand selection.

The importance of protein dynamics in controlling the access and binding of ligands has long been recognized (e.g., induced fit model), but only recently methods have become feasible that utilize this property for virtual drug screening.[40] The NMR dynamics data presented here are uniquely suited for this purpose as they demonstrate the differential response of the N-terminal lid to various ligands and the lid's ability to directly interfere with ligand binding to the hydrophobic cleft. Incorporation of the lid properties into drug design and virtual screening should therefore help to improve the binding efficacy of the next generation of rationally designed inhibitors of MDM2.

Acknowledgment. S.A.S. is the recipient of an NIH post doctoral fellowship. E.J. is the recipient of an American Heart Association postdoctoral fellowship. We thank Dr. Michael Bubb

(37) Stoll, R.; Renner, C.; Muhlhahn, P.; Hansen, S.; Schumacher, R.; Hesse, F.; Kaluza, B.; Engh, R. A.; Voelter, W.; Holak, T. A. *J. Biomol. NMR* **2000**, *17*, 91–92.
(38) Fry, D. C.; Graves, B.; Vassilev, L. T. *Ubiquitin and Protein Degradation, Pt B* **2005**, *399*, 622–633.
(39) Grasberger, B. L. et al. *J. Med. Chem.* **2005**, *48*, 909–912.
(40) Carlson, H. A.; McCammon, J. A. *Mol. Pharmacol.* **2000**, *57*, 213–218.

for performing the analytical ultracentrifugation experiments. This work was supported by National Science Foundation Grant 0621482. The NMR experiments were conducted at the National High Magnetic Field Laboratory (NHMFL) supported by cooperative agreement DMR 0654118 between the NSF and the State of Florida.

Supporting Information Available: Six figures presenting chemical shift and relaxation data, complete refs 23 and 39. This material is available free of charge via the Internet at http://pubs.acs.org.

JA800201J